Petroleum Science 23 (2026) 5189–5202

Contents lists available at ScienceDirect

Petroleum Science

journal homepage: www.keaipublishing.com/en/journals/petroleum-science

Original Paper

# Flocculation–microfiltration integration for high-salinity oilfield offshore produced water treatment

Mariane Carolina Proner [a,b], Maria Alice Prado Cechinel [a,b], Carine Loureço Alves [a,b], Sálvio Lima de Carvalho Neto [a,c], Silvio Edegar Weschenfelder [d], Sergio Yesid Gómez González [c], Alan Ambrosi [b], Marco Di Luccio [b], Regina de Fatima Peralta Muniz Moreira [a,*]

[a] Laboratory of Energy and Environment, Department of Chemical and Food Engineering, Federal University of Santa Catarina, Florianópolis, 88040-970, Santa Catarina, Brazil
[b] Laboratory of Membrane Processes, Department of Chemical and Food Engineering, Federal University of Santa Catarina, Florianópolis, 88040-970, Santa Catarina, Brazil
[c] Laboratory of Mass Transfer and Numerical Simulation of Chemical Systems, Department of Chemical and Food Engineering, Federal University of Santa Catarina, Florianópolis, 88040-970, Santa Catarina, Brazil
[d] Petrobras Research Center, Rio de Janeiro, 21941-915, Rio de Janeiro, Brazil

ARTICLE INFO

*Article history:*
Received 3 November 2025
Received in revised form
16 December 2025
Accepted 11 March 2026
Available online 14 March 2026

Edited by Min Li

*Keywords:*
Ceramic membrane
Dispersed oil
Fouling mechanisms
Produced water treatment
High-salinity wastewater

ABSTRACT

This study evaluated an integrated treatment system that combines chemical destabilization (through flocculation) with membrane-based separation (via submerged microfiltration) for removing of dispersed oil from oilfield produced water (OPW) under realistic salinity and temperature conditions. Both synthetic and real OPW emulsions were treated using polymeric flocculants, followed by the submerged-MF employing 0.1 μm tubular and flat sheet ceramic membranes at 60 °C. System performance was assessed in terms of total oil and grease (TOG) removal and permeate flux. Fouling mechanisms were analyzed using Hermia models alongside a Python®-based numerical simulation, fitting the empirical resistance decay via nonlinear optimization. The use of the commercial anionic flocculant HYPERFLOC™ AE 120 led to TOG removal efficiencies up to 85% in synthetic emulsions prepared with 100 g/L NaCl at 60 °C. The integrated flocculation/submerged-MF process ensured full compliance with offshore discharge regulations for produced water. Membrane configuration strongly influenced performance; flat sheet membranes exhibited milder flux decline and superior flux recovery after cleaning, while tubular membranes were prone to pore-blocking. In contrast, cake layer formation was more prominent in flat membranes. Empirical exponential decay models provided the best fit for resistance evolution ($R^2 = 0.996$), surpassing the accuracy of the mechanistic Hermia models in describing fouling behavior. For oilfield produced water emulsions, flocculation was less efficient due to the matrix complexity. However, submerged-MF significantly reduced TOG content and turbidity. Overall, the engineered integrated system demonstrated robustness and scalability potential for OPW treatment in challenging offshore environments, highlighting the benefits of process synergy and operational adaptability.



## 1. Introduction

Oilfield produced water (OPW) is the main byproduct of offshore oil and gas extraction, with increasing production over recent decades and an estimated global volume of around 250 million barrels per day (Shahrim et al., 2023). It is a highly complex oily aqueous matrix whose composition varies depending on the geological features of the reservoir and the exploration phase. Generally, it contains aliphatic and aromatic hydrocarbons,

* Corresponding author.
*E-mail address:* regina.moreira@ufsc.br (R.F. Peralta Muniz Moreira).
Peer review under the responsibility of China University of Petroleum (Beijing).

https://doi.org/10.1016/j.petsci.2026.03.025
1995-8226/

phenols, organic acids (Hu et al., 2025), as well as dissolved solids, metal ions, chemical additives used during extraction, and high salinity (up to ten times that of seawater in some areas) (Ariana et al., 2025; Tian et al., 2023).

Conventional produced water treatment involves several stages, such as three-phase separators, hydrocyclones, and flotation processes. Its main goal is to lower the total oil and grease (TOG) levels, which in wastewater are found both as dispersed oil micro-droplets and dissolved, particularly as water-soluble organics (WSO). The treatment's purpose is to comply with regulatory discharge limits—typically under 30 mg/L of TOG – and to mitigate environmental impact while protecting marine ecosystems (Amakiri et al., 2022; Bostick, 2002; Dai et al., 2023).

While traditional methods are commonly used on production platforms, alternative approaches such as microfiltration (MF) are gaining extensive interest for treating produced water. This technique is particularly aimed at separating the emulsified oil phase from the water phase (Liu et al., 2021; Padaki et al., 2015; Zhang et al., 2022). The pursuit of more effective solutions is driven by the varying complexity of OPW and the likelihood of stricter environmental regulations in the future. Typically, MF can remove microscopic particles (less than 5 μm), including stable emulsions, without relying on chemical additives or thermal processes limitations often associated with current methods used on platforms for oil separation (Wang et al., 2023).

In this context, submerged membrane microfiltration (submerged-MF) stands out as a promising, and underexplored alternative for treating OPW. In this setup, the membrane is immersed directly in the wastewater, with filtration driven by moderate vacuum applied on the permeate side (Jin et al., 2019). This design enables operation at lower transmembrane pressure (TMP) and requires a smaller footprint, making it ideal for the space-constrained environments of the offshore platforms (Al-Shammari et al., 2012; Jin et al., 2019; Motta et al., 2014; Piombini et al., 2021). Thus, submerged-MF offers significant advantages over traditional pressurized systems, particularly for applications in offshore facilities, where space is typically limited.

Furthermore, submerged-MF can be integrated into existing flotation/flocculation stages on platforms, which serve as pre-treatment, helping to reduce fouling and extend membrane lifespan, thus promoting a promising integrated process for OPW treatment, especially in offshore units. Flocculation is especially effective at removing colloidal material from oily wastewater by forming flocs through charge neutralization and reducing electrostatic repulsion in the electrical double layer (Zhao et al., 2021). When combined with MF, flocculation acts as the first step, removing larger particles and oil droplets, while MF then filters the remaining smaller oil droplets under μm.

Specific characteristics of OPW and offshore conditions, along with operating parameters, must be considered when optimizing the flocculation/MF process. For instance, the salinity of OPW affects the surface charge of oil droplets, directly impacting separation efficiency (Wang et al., 2022), and lead to membrane fouling (Jiménez et al., 2018). Temperature is another factor that must be considered, as OPW can reach temperatures of up to 92 °C (Alzahrani and Mohammad, 2014). Variations in temperature can influence viscosity, interfacial tensions, solubility of components present in the produced water, and the frequency of oil droplet coalescence (Piccioli et al., 2020). Additionally, chemical additives can alter droplet charge, decrease electrostatic repulsion, and promote adhesion to gas bubbles, thereby improving flocculation efficiency (Yang et al., 2016).

This study investigated a novel integrated process combining flocculation and submerged-MF to remove dispersed oil from OPW under challenging conditions of high salinity (100 g/L NaCl) and elevated temperature (up to 60 °C). Bench-scale experiments were conducted as a proof-of-concept (Technology Readiness Level 3-TRL 3). A numerical simulation framework was developed to analyze flux decline mechanisms during membrane filtration. This model employs finite difference discretization to evaluate mass transport across the membrane, accounting for both axial and radial concentration profiles under transient conditions. Experimental flux decay data were fitted using in-house Python®-based optimization routines to assess key fouling model parameters, allowing comparison among Hermia, exponential decay, power law, and logistic models.

By incorporating initial flux, membrane configuration, and empirical decay expressions, the simulation provided valuable insights permeate flux decline over time, supporting the interpretation of fouling mechanisms and the design of CFD boundary conditions for computer-based simulations and optimization. The novelty of this work lies in the integration of flocculation and MF for OPW treatment under conditions representative of offshore production environments. The findings aim to enhance the technological readiness of the proposed approach and support its future scale up and implementation on offshore platforms.

## 2. Methods

### 2.1. Preparation and characterization of dispersed oil emulsions in synthetic and real produced water

Synthetic produced water with dispersed oil (SPW-DO) was prepared by emulsifying crude oil, sourced from an offshore exploration unit on the Brazilian coast, within a saline matrix. This matrix consists of a 100 g/L NaCl solution in distilled water, with the pH monitored using a benchtop pH meter (AZ 86505), and adjusted to a range of 5 to 7 using either HCl (Neon P.A. ACS, 37% and 1 mol/L solution) or 2 mol/L NaOH solution (Êxodo Científica P.A. ACS).

The emulsion was prepared in a 2 L glass beaker containing 1.5 L of the saline matrix, which had been preheated to 60 °C in a thermostatic bath. Once the target temperature was reached, approximately 1.0 g of crude oil was slowly added under constant stirring, using an Ultra-Turrax disperser (IKA®) operating at 12,000 rpm for 15 min. The temperature was maintained at 60 °C throughout the entire process. The crude oil used in the experiment had a specific gravity of 913 $kg/m^3$ and a viscosity of 116.8 mPa·s at 25 °C. Upon completion of emulsification, the mixture was transferred to an oven (New Lab), also kept at 60 °C, and let stand for 30 min to allow the separation of the free (non-emulsified) oil phase. The emulsion was then carefully collected from the lower side outlet of the beaker and used in subsequent tests. This method enables the preparation of an aqueous matrix with dispersed oil, featuring a TOG content between 100 and 150 mg/L, as described by Scharnberg et al. (2023).

In addition to the synthetic matrix, a real produced water sample, collected from the outlet of the flotation stage at an offshore oil production unit, was used to prepare a real matrix of produced water emulsion containing dispersed oil (OPW-DO). The salinity of the matrix was adjusted to 100 g/L, and the pH was set between 6 and 8. Subsequently, 0.7 g of crude oil was emulsified using the Ultra-Turrax disperser, operating at 12,000 rpm for 5 min, while maintaining the temperature at 60 °C. After emulsification, the mixture was allowed to rest in an oven at 60 °C for 30 min to promote the separation of the free oil phase. The resulting emulsion, with a TOG content between 100 and 150 mg/L, was collected from the bottom outlet of the beaker and used in the subsequent experiments. The OPW-DO preparation required a shorter homogenization time (5 min) than the synthetic matrix (15 min) to achieve the target TOG, probably due to the presence of naturally occurring compounds in the real matrix, such as surfactants, that facilitated faster emulsion formation.

The quantification of TOG content in both SPW-DO and OPW-DO samples was carried out using non-dispersive infrared spectroscopy with a Horiba® OCMA 350 instrument. For this purpose, a calibration curve was constructed by dissolving known masses of crude oil in tetrachloroethylene (CAS 127-18-4, Êxodo Científica P.A.), resulting in a range of oil concentrations (mg/L), as described by Scharnberg et al. (2023). For the analysis, 50 mL of each sample was acidified to pH 2.0 with 37% HCl and subjected to liquid-liquid extraction with a total of 15 mL of tetrachloroethylene organic solvent, applied in three sequential steps.

In the first extraction step, 5 mL of solvent was added to the acidified sample, agitated for 2 min, and allowed to rest for 5 min to facilitate phase separation. The denser organic phase was separated, filtered through a separatory funnel containing a layer of anhydrous sodium sulfate, and collected in a glass flask. This procedure was repeated twice, each time using 5 mL of fresh solvent and following the same protocol. All collected organic phases were combined in the same glass flask for subsequent analysis. With the aid of the calibration curve, TOG content (mg/L) was quantified using Eq. (1):

$$\mathrm{TOG} = \frac{1}{\tan\theta} \times \mathrm{Abs} \times \frac{V_\mathrm{b}}{V_\mathrm{a}} \quad (1)$$

in which, $\tan\theta$ represents the slope of the calibration curve, which is derived from the calibration process. Abs refers to the absorbance of the sample as measured by the spectrophotometer. $V_\mathrm{b}$ denotes the total volume of the solvent utilized during the extraction process, and $V_\mathrm{a}$ is the volume of the sample that was subjected to extraction.

Turbidity was measured using a benchtop turbidimeter (Hanna, HI98703). The salinity of the OPW-DO and SPW-DO samples was determined with a refractometer (ATC model). Total solids (TS), fixed solids (FS), and volatile solids (VS) were quantified according to SM 2540 methodologies (APHA, 2017). Zeta potential ($\zeta$) measurements were performed using a Malvern® Zetasizer Nano ZS for the SPW-DO emulsion and for the flocculant solutions prepared at the concentrations used in the tests and dissolved in distilled water. All measurements were carried out in triplicate at $\mathrm{pH} = 6.5$. The determination of the zeta potential of the flocs formed after the addition of surfactant and flocculant was not feasible due to the formation of large, sticky aggregates that hindered sample handling and prevented proper loading into the analytical cell of the instrument.

Droplet size distribution was evaluated by capturing images with an optical microscope (Olen) at magnifications of 100x, 400x, and 1000x, followed by image analysis using ImageJ software. Statistical parameters such as $D_\mathrm{mode}$ and $D_\mathrm{mean}$ were calculated directly in Microsoft Excel® using the corresponding functions, based on the droplet dataset measured for each emulsion. $D_\mathrm{mean}$ corresponds to the arithmetic mean diameter, whereas $D_\mathrm{mode}$ represents the most frequent droplet diameter in the distribution (i.e., the statistical mode). The Sauter mean diameter ($D_\mathrm{Sauter}$), defined as the surface-area-weighted mean droplet diameter, was also derived from the droplet size distribution. Conceptually, $D_\mathrm{Sauter}$ represents the diameter of a spherical droplet with the same volume-to-surface-area ratio as the entire droplet population. Because smaller droplets contribute proportionally more surface area per unit volume, they exert a greater influence on $D_\mathrm{Sauter}$ than on $D_\mathrm{mean}$.

### 2.2. Flocculation tests of SPW-DO with different flocculating agents

Flocculation tests on the SPW-DO (synthetic produced water with dispersed oil) were performed using several polymeric flocculants commonly employed in offshore produced water treatment units. The polymers tested included: HYPERFLOC™ CE 814, HYPERFLOC™ CB 482, and HYPERFLOC™ AE 120, with their physicochemical characteristics listed in Table 1.

Flocculation tests were performed using a Jar Test apparatus (Nova Ética). Each test involved placing 400 mL of SPW-DO, prepared as described in section 2.1, into 1.0 L beakers. To simulate the conditions of actual produced water samples, which often include surfactants from extraction processes, SBDS surfactant was added to the SPW-DO to achieve a final concentration of 200 mg/L. The mixture was then stirred at 100 rpm for 2 min. Subsequently, the polymer under investigation was added to reach a final concentration of 85 mg/L. These concentrations were selected based on the study by Scharnberg et al. (2023) and preliminary experimental results.

After adding polymer, the mixture underwent rapid agitation at 150 rpm for 30 s, then switched to slow flocculation at 50 rpm for 10 min. Once flocculation was complete, samples were left undisturbed for 50 min to allow flocs to settle. The clear aqueous phase was then carefully decanted for further analysis of TOG content via spectrophotometry (Horiba® OCMA 350) and turbidity measurements. All experiments were performed in triplicate.

### 2.3. Integration of flocculation and submerged microfiltration processes in SPW-DO treatment

#### 2.3.1. Evaluation of flocculant concentration and membrane configuration

The performance of the flocculation process followed by submerged microfiltration (submerged-MF) in reducing TOG content was evaluated under different flocculant application scenarios. The SPW-DO used was prepared as described in Section 2.1. Flocculation was conducted using a bench-scale system. This system comprised a 2 L saturator vessel equipped with a pressure gauge, relief valve, and needle valve. It was connected to a 1.8 L jacketed glass vessel with a benchtop mechanical stirrer (Fisatom®) and a thermostatic circulation bath (Sevenlabor). The system also included a control point for operational pressure.

For all flocculation tests, 1.2 L of SPW-DO was transferred to the jacketed glass vessel and maintained at a constant temperature of 60 °C. Three flocculation conditions were tested, varying the surfactant concentrations (100, 150, and 200 mg/L) and the previously selected flocculant polymer (chosen for its optimal performance) at 50, 75, and 100 mg/L. First, the surfactant was added to the heated solution at the specified concentrations, and agitation was maintained at 250 rpm for 2 min. Next, the flocculant polymer was added, and agitation was increased to 350 rpm for 30 s. This was followed by a slow agitation at 60 rpm until a total of 10 min was reached. After the agitation, the samples remained at rest in the jacketed vessel, still at 60 °C, for 50 min, allowing the formed flocs to separate. At the end of this period, the liquid phase was carefully collected via the lower side valve of the vessel.

**Table 1**
Physicochemical properties of employed polymeric flocculants.

| | CE 814 | CB 482 | AE 120 |
|---|---|---|---|
| Charge | Cationic | Anionic | Anionic |
| Charge density | Medium | High | N.R. |
| Specific density, g/cm$^3$ | 1–1.1 | 1.05–1.15 | 1–1.1 |
| Viscosity, cP | 500–200 | <500 | <50 |
| Non-Volatile Solids Content, % | 37.5–44.5 | 18–23 | 17–19 |
| Zeta potential ($\zeta$) at pH = 6.5, mV | 3.57 | −3.70 | −7.93 |

N.R.: Not reported.

The samples obtained under each flocculation condition were subjected to the submerged-MF process, using the same jacketed glass vessel employed in the previous step, maintained at 60 °C. Two single-channel tubular ceramic membranes (alumina-based, porosity 40%, pore size of 0.1 μm, and a total filtration area of 79.2 $cm^2$) were submerged in the sample and operated in parallel. The permeation process was conducted under vacuum pressure of 0.1 bar, using a gear pump (Cole-Parmer, 75211-62), for approximately 1.5 h. During this period, the permeate volume was continuously collected and measured.

The TOG content of the initial SPW-DO samples, as well as after flocculation and after submerged-MF, was measured by spectrophotometry, as described in Section 2.1. The permeate flux ($J$) was calculated using Eq. (2), based on the permeate volume ($V_p$) collected over time ($t$) and the effective membrane filtration area ($A$). The specific permeate flux ($J_e$), a dimensionless quantity, was determined by dividing the measured flux ($J$) by the flux measured with permeation using only distilled water ($J_w$), as shown in Eq. (3).

$$J = \frac{V_p}{t \times A} \tag{2}$$

$$J_e = \frac{J}{J_w} \tag{3}$$

At the end of each test, the membranes underwent a standardized cleaning procedure of four sequential steps, each performed at 60 °C for 20 min: (i) rinsing with distilled water, (ii) alkaline cleaning with a 0.5% NaOH solution; (iii) acidic cleaning with a 2.0% citric acid solution, and (iv) a final rinse with distilled water.

To assess the impact of membrane configuration on system's efficiency in reducing TOG content, a multi-channel flat ceramic alumina membrane, with effective area of 60 $cm^2$ and a pore size of 0.1 μm, was also used and compared to the tubular membrane. Flocculation conditions were maintained at constant concentrations of 150 mg/L surfactant and 75 mg/L flocculant polymer, following the protocol outlined in the preceding section. After flocculation, the sample was filtered using submerged-MF. The only modification from previous tests was the replacement of the tubular membranes with the flat membrane, while all other operational conditions remained unchanged. The permeate volume was collected and monitored for approximately 1.5 h, enabling a direct comparison of performance between the different membrane geometries.

### 2.3.2. Membrane performance assessment and fluid dynamic simulation

The Hermia model was employed to characterize and simulate the flux in the two membranes studied. Hermia's model is widely used in fouling analysis of porous membranes, providing a theoretical framework to explain the decrease in permeate flux over time due to the accumulation of foulants on the membrane surface or within its pores (Abbasi et al., 2012; Pereira et al., 2023). This phenomenological model considers four primary fouling mechanisms: complete pore blocking, intermediate (or partial) pore blocking, standard blocking, and cake layer formation (Pereira et al., 2023). Each mechanism corresponds to a characteristic exponent in the flux equation, enabling Hermia's model not only to quantify the fouling rate but also to infer the dominant fouling behavior during the filtration (Hermia, 1985). The model equations are presented in Supplementary Material Section S1.

Analyzing the fit of experimental data to different regimes of the Hermia model aids in identifying the dominant fouling mechanism and understanding how membrane-fluid interactions contribute to permeability reduction. To facilitate this analysis, an optimization algorithm was developed to evaluate the fit of the proposed model equations. Additionally, a custom simulation code, developed in Python®, was used to predict fouling dynamics within the membrane filtration system. This model employs a finite volume scheme to describe species transport and membrane flux decay in both configurations, discretized along both radial and axial directions. Membrane behavior is modeled by a time-dependent decline in permeate flux, enabling simulation of both the initial clean flux and its reduction due to fouling. The flexible structure of the code enables dynamic manipulation of critical membrane parameters, including the rate of permeate flux decay, fouling onset delay, and species-specific interactions. Experimental water flux data were fitted by optimizing the initial permeate flux and decay rate using a bounded nonlinear optimization routine.

To simulate permeate flux decline in the APOD membrane system, a custom finite volume code was developed in Python®. The model resolves transient species transport through both systems, discretized in radial and axial directions. Fouling is incorporated as a time-dependent permeability decay function, applied independently to water and oil based on empirical trends and literature-informed behavior. An initial analysis was performed using the Hermia models (detailed in the Supplementary Material) was performed to characterize the observed flux decline. Additionally, empirical decay models from the literature, including the power law, exponential, and logistic models (Bhattacharya et al., 2010; Field et al., 1995; Sutzkover-Gutman et al., 2010), were evaluated to capture non-mechanistic trends in the resistance for the proposed custom-developed finite volume code. A comprehensive description of these equations is provided in Table S2 (Supplementary Material).

The optimization process minimized the weighted squared error between the simulated and experimental normalized flux. Membrane domain discretization was achieved using finite volume grids ($N_r = 25$, $N_z = 50$), with time steps dynamically governed by diffusion stability criteria. Optimization of the initial permeate flux and decay rate was performed using a bounded nonlinear optimization routine (*scipy.optimize.minimize*), employing both the 'L-BFGS-B' and 'TNC' algorithms with tolerance of $1 \times 10^{-6}$ and a maximum of 1000 iterations. All fitting and simulation procedures were validated by comparing the predicted flux trends to experimental data, as discussed further. On average, the simulations took 151.2 s for the tubular membrane and 192.5 s for the flat membrane, demonstrating the code's potential for rapid prediction of fouling mechanisms.

## 2.4. Integration of flocculation and submerged microfiltration processes in OPW-DO treatment

Flocculation tests with OPW-DO were conducted under fixed conditions, using 200 mg/L of SBDS and 100 mg/L of AE 120, following the procedure detailed in Section 2.3.1. Permeation experiments were performed using both the flat ceramic membrane (alumina-based, porosity 40%, pore size of 0.1 μm, and a total filtration area of 60 $cm^2$) and the tubular alumina ceramic membrane used in previous tests (alumina-based, porosity 40%, pore size of 0.1 μm, and a total filtration area of 79.2 $cm^2$). The permeate volume was collected and monitored over a period of approximately 1.5 h, enabling a direct comparison of performance between the two membrane configurations under identical operational conditions.

The samples obtained at this stage of the study, both prior to and following flocculation and submerged-MF, were characterized for TOG content via liquid-liquid extraction with tetrachloroethylene, as well as for turbidity, total solids (TS), fixed solids (FS), and volatile solids (VS), as described in Section 2.1. The droplet size distribution of the OPW-DO emulsion was determined from images obtained using optical microscopy (Olen) and analyzed using ImageJ software.

## 3. Results and discussion

### 3.1. Dispersed oil (DO) emulsions characterization: synthetic (SPW-DO) and oilfield produced water (OPW-DO)

The real aqueous matrix (i.e. real produced water) exhibited a salinity of 22 g/L, as determined using a refractometer, and a turbidity of 7.88 NTU. The concentration of total suspended solids (TSS) was 23.7 ± 0.2 mg/L, of which 19.21 ± 0.04 mg/L corresponded to fixed solids. To standardize the salt content across different matrices and enable a reliable comparison in emulsion preparation and floc formation, NaCl was added to the real matrix prior to the preparation of the OPW-DO emulsion, resulting in a final salinity of 101 g/L. In this adjusted matrix, the TSS concentration was equal to 96.4 ± 0.3 mg/L (91.39 ± 0.04 mg/L of fixed solids). This adjustment allowed direct comparison with the emulsion prepared using distilled water and salt (SPW-DO), which had a salinity of 100 g/L. The pH of all samples used in this study ranged from 5.0 to 7.5.

Table 2 summarizes the physicochemical characteristics of each water matrix, while Fig. 1 presents the histograms of droplet size distribution for both SPW-DO and OPW-DO, along with 40x magnified digital images of the oil droplets dispersed in water.

The OPW-DO and SPW-DO were prepared using identical operating conditions (12,000 rpm, pH between 5.0 and 7.5, and a temperature of 60 °C), but with different homogenization times. The combination of this shorter mixing time and complex composition of the real matrix resulted in emulsions with distinct characteristics. The OPW-DO exhibited higher turbidity (924 NTU) and TOG concentrations (154 ± 22 mg/L) compared to SPW-DO (477 NTU and 114 ± 16 mg/L, respectively). These results indicate a higher pollutant load and a greater presence of fine suspended particles in the real matrix.

Regarding the oil droplet size distribution, OPW-DO showed larger droplets compared to SPW-DO (Table 2). This difference in droplet size can be partially attributed to the variation in stirring time during emulsion preparation. While SPW-DO underwent 15 min of mixing, OPW-DO was emulsified for only 5 min, both using the same dispersing equipment. Even so, based on the droplet size distribution, both emulsions can be classified as oil-in-water emulsions with droplet sizes ranging from 1 to 10 μm (Kim et al., 2019; Li et al., 2025).

**Table 2**
Comparison of preparation conditions, physicochemical parameters, and droplet size of the SPW-DO and OPW-DO emulsions. OPW-DO required a shorter preparation time due to emulsion-forming compounds present in the aqueous matrix.

| Parameters | SPW-DO | OPW-DO |
|---|---|---|
| Aqueous matrix | Distilled water | Real produced water |
| Ultraturrax velocity, rpm | 12,000 | 12,000 |
| pH | 5.0–7.5 | 5.0–7.5 |
| $T$, °C | 60 | 60 |
| Agitation time, min | 15 | 5 |
| Total oil and grease (TOG), mg/L | 114 ± 16 | 154 ± 22 |
| Turbity, NTU | 477 | 924 |
| Salinity, mg/L | 100 | 101 |
| $D_{\text{max}}$, μm | 3.45 | 5.97 |
| $D_{\text{min}}$, μm | 0.16 | 0.57 |
| $D_{\text{mean}}$, μm | 1.01 | 1.54 |
| $D_{\text{mode}}$, μm | 1.17 | 1.01 |
| $D_{\text{Sauter}}$, μm | 0.71 | 1.16 |

Longer mixing times, particularly when using high-shear equipment, promote droplet breakup and lead to finer, more uniform emulsions, thus, the shorter mixing time applied to OPW-DO may have contributed to the formation of larger droplets and a less uniform emulsion. This behavior is corroborated by the histogram in Fig. 1(b), which displays a concentration of droplets around the mode ($D_{\text{mode}}$ = 1.01 μm), with fewer occurrences of larger droplets ranging from 2 to 5 μm in diameter. The $D_{90\%}$ value, representing the diameter below which 90% of the droplet volume is contained, was significantly higher for OPW-DO (<3.14 μm) than for SPW-DO (<1.66 μm), indicating greater heterogeneity in droplet size distribution.

Separation efficiency in flocculation processes is influenced by several factors, including oil droplet diameter (Taghizadeh Mohammadi and Movahedirad, 2024), and generally decreases as the average droplet size becomes smaller. Ultrafine droplets exhibit reduced coalescence potential and diminished buoyancy (Shim et al., 2025). Consequently, the complete removal of such droplets often necessitated the use of chemical additives that facilitate their aggregation.

### 3.2. Flocculation tests of SPW-DO with different flocculating agents

Fig. 2 presents the TOG concentrations and turbidity measurements obtained from flocculation tests conducted on the SPW-DO emulsion with three distinct flocculants: Hyperfloc AE 120, CB 482, and CE 814. Although limited technical specifications are provided by the manufacturer for these commercial products, they are widely employed in offshore oil platform operations as well as in water and wastewater treatment applications. Hyperfloc AE 120 and Hyperfloc CB 482 contain anionic active ingredients, whereas Hyperfloc CE 814 contains a cationic active ingredient. The zeta potential values of the flocculants (Table 1) also reflect their inherent surface charge characteristics at the working pH around 6.5. CE 814 exhibited a slightly positive $\zeta$-potential, consistent with its cationic functionality, whereas CB 482 and AE 120 showed negative $\zeta$-potentials, in agreement with their anionic nature.

The results highlight the effectiveness of the various polymeric flocculants in reducing turbidity and TOG concentration, with their differing performances attributed to specific physicochemical properties and interaction with oil droplets in the aqueous medium. CE 814, the sole flocculant containing a cationic active component, exhibited the lowest efficiency among the tested polymers, achieving reductions of 84% in turbidity and 81% in TOG concentration. Its poor performance, however, is not only related to the fact that it is cationic, but also to the presence of 200 mg/L of surfactant and 100 g/L of NaCl, which hinder its adsorption at the oil-water interface and suppress electrostatic mechanisms (Khan et al., 2018). In contrast, the anionic flocculants, AE 120 and CB 482, demonstrated superior performance. AE 120 achieved a 94% reduction in turbidity and an 85% reduction in TOG, whereas CB 482 reduced turbidity by 93% and TOG by 73%, resulting in an average final TOG concentration of 33 mg/L. Among the tested flocculants, AE 120 presented the most effective destabilization, producing visibly larger and more compact flocs and yielding a completely translucent supernatant. In comparison, CE814 generated small, fragile flocs and a noticeably turbid supernatant, while CB482 produced intermediate behavior.

These results allow us to infer the flocculation mechanisms that operate in this system for each flocculant used. Under low or zero salinity conditions, oil droplets typically exhibit negative surface charges resulting from the preferential adsorption of hydroxide

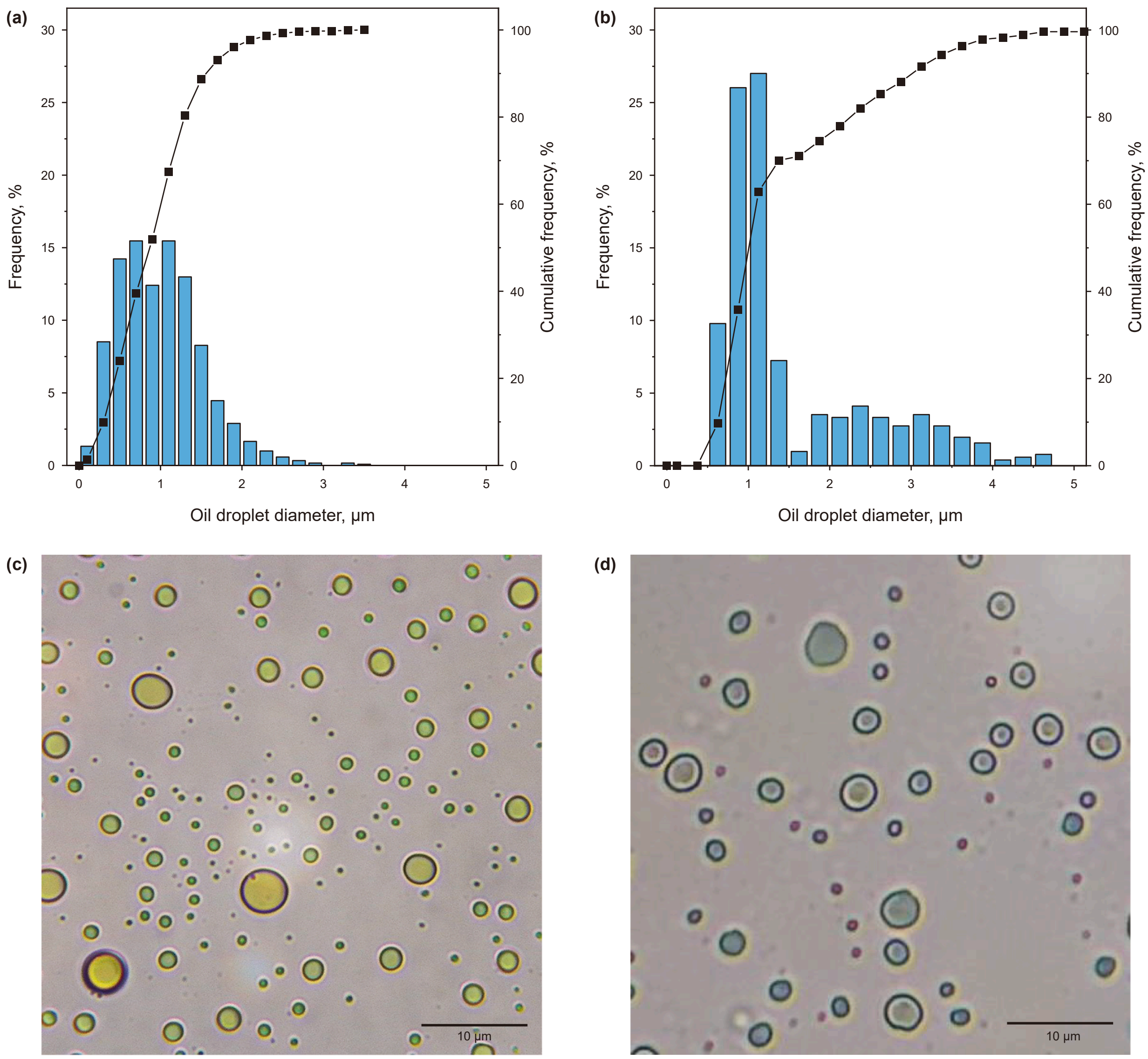


**Fig. 1.** Histogram of oil droplet size distribution for the emulsions: **(a)** SPW-DO (1209 droplets) and **(b)** OPW-DO (511 droplets); digital image of oil droplets in emulsions **(c)** SPW-DO magnified 100x and **(d)** OPW-DO magnified 40x.

ions at the oil-water interface (Wang et al., 2022). In such scenarios, cationic polymers are effective due to their dual role in aggregation and flocculation, that is, they neutralize the negative surface charge on the droplets, thereby promoting floc formation and phase separation (Zhao et al., 2021) (Fig. 3(a)).

Conversely, under high salinity conditions, oil droplets may undergo either charge inversion or partial neutralization (Dudek and Øye, 2018), which makes anionic or nonionic polymers more suitable for promoting aggregation of oily droplets (Fig. 3(b)). In the present study, the high ionic strength of the SPW-DO matrix compresses the electrical double layer, thereby reducing the magnitude of the zeta potential and partially neutralizing the surface charge of the oil droplets (Huang et al., 2019). As a result, the droplets exhibit only weak electrostatic repulsion ($\zeta = -6.37$ mV), indicating minimal electrostatic stabilization. This partial charge neutralization, coupled with extensive electrostatic screening, confirms that electrostatic interactions play a negligible role under these conditions. This evidence strongly supports the interpretation that flocculation is predominantly governed by hydrophobic interactions and polymer bridging, rather than by charge neutralization mechanisms (Scharnberg et al., 2023).

Based on these results and considering its superior performance in reducing TOG concentration and turbidity under saline conditions, the flocculant AE 120 was selected for subsequent experiments and will hereafter be referred to as [AE].

### 3.3. Integrating flocculation and submerged microfiltration in PW-DO treatment

#### 3.3.1. Evaluation of flocculant agent concentration

To assess the performance of ceramic membranes under varying oil concentrations, flocculation conditions were modified by adjusting the concentration of [AE] across three independent tests. This approach enabled generation of different flocculation efficiencies and, consequently, varying oil concentrations in the feed stream to the membrane unit. The results for TOG concentrations and permeate flux obtained in each test are presented in Fig. 4.

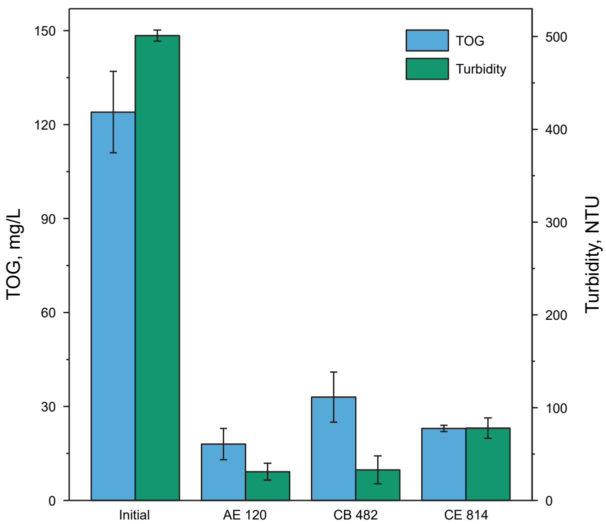


**Fig. 2.** Performance of the different flocculants in SPW-DO treatment. TOG content (mg/L) and turbidity (NTU). Experimental conditions ($n$ = 3): $T$ = 60 °C, [flocculant] = 85 ± 2 mg/L, [surfactant] = 200 ± 5 mg/L, and [NaCl] = 100 g/L.

In the test conducted with 50 mg/L of [AE], flocculation reduced TOG concentration by 22% (from 125 to 98 mg/L), as illustrated in Fig. 4(a). The subsequent microfiltration step enhanced the overall TOG removal to 94%, achieving a final concentration of 7 mg/L, thereby demonstrating the membrane's capacity to compensate for suboptimal flocculation performance. At [AE] concentrations of 75 and 100 mg/L, flocculation alone removed more than 83% of the oil, resulting in low residual oil concentrations in the membrane feed. In these cases, MF functioned primarily as a polishing step to conventional treatment. Although small variations in permeate TOG were observed among the flocculant doses, these differences were not statistically significant (ANOVA, $p > 0.05$), indicating that the submerged-MF step produced comparable TOG levels regardless of the flocculant concentration.

The effectiveness of integrated system is likely associated with two primary mechanisms that govern the treatment of oil-in-water (O/W) emulsions using membrane technology: (1) coalescence, wherein dispersed oil droplets merge upon contact with the membrane surface, and (2) size exclusion, whereby droplets exceeding the membrane pore size are physically retained. These mechanisms act synergistically, facilitating the efficient separation of O&G compounds and suspended solids (Zolfaghari et al., 2016).

Analysis of specific permeate flux analysis (Fig. 4(b)) revealed minimal dependence on O&G concentration post-flocculation. This behavior was particularly evident in the test with 50 mg/L of flocculant, where the membrane feed contained 100 mg/L O&G, approximately 75% higher than in the tests with 75–100 mg/L of flocculant. The stable flux values indicate that oil-induced fouling was mitigated through interfacial coalescence, enlargement of oil droplets beyond the membrane pore size, and the hydrophilic barrier effect, where the ceramic membrane's hydrophilicity promotes the formation of a surface hydration layer that repels apolar compounds.

These findings indicate that the performance of the integrated system is more sensitive to flocculant dosage than to residual oil concentration when the system operated under sub-critical flux conditions (i.e., mild operating pressures). At the lowest flocculant dosage (50 mg/L), TOG reduction was limited, suggesting that the negative charge density was insufficient to induce effective emulsion destabilization. In contrast, flocculant concentrations in the 75 to 100 mg/L range yielded maximum efficiency, indicating an optimal flocculation concentration. These results suggest that 75 mg/L represents the optimal dosage, as further increases in flocculant do not improve separation efficiency and indicate a saturation of aggregation mechanisms. Even under moderate flocculation efficiencies (22%–83%), the system maintained stable filtration performance, highlighting its potential as an effective tertiary treatment stage. Importantly, the integrated system produced effluent containing less than 30 mg/L of O&G, meeting offshore discharge regulatory standards.

### 3.3.2. Evaluation of membrane configuration

Fig. 5 shows the results of the performance evaluation of tubular and flat sheet membrane configurations applied to the combined treatment of SPW-DO, integrating flocculation followed by submerged-MF.

Both tests exhibited a pronounced decline in the specific permeate flux over time (Fig. 5(a)). Specific flux analysis revealed that the tubular membrane operated at approximately 12% of its initial flux by the end of the test, whereas the flat sheet membrane maintained about 17%. This outcome suggests a reduced tendency for severe flux decline in the flat sheet configuration, despite its lower initial absolute flux values. Another relevant aspect pertains to flux recovery following chemical cleaning. The initial flux if the flat sheet membrane with distilled water was 900 L/(m$^2$·h), and it remained virtually unchanged after cleaning (905 L/(m$^2$·h)). In contrast, the tubular membrane exhibited an expressive flux reduction, decreasing from 803 L/(m$^2$·h) before operation to 487 L/

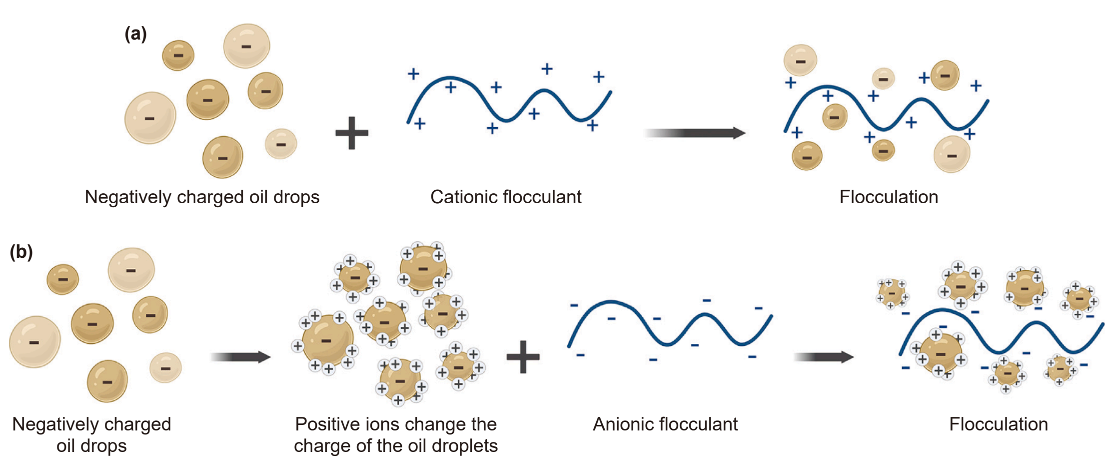


**Fig. 3.** Proposed mechanism for the flocculation of crude oil emulsions by cationic and anionic polymers in saline media (adapted with permission from Georgie (2024)).

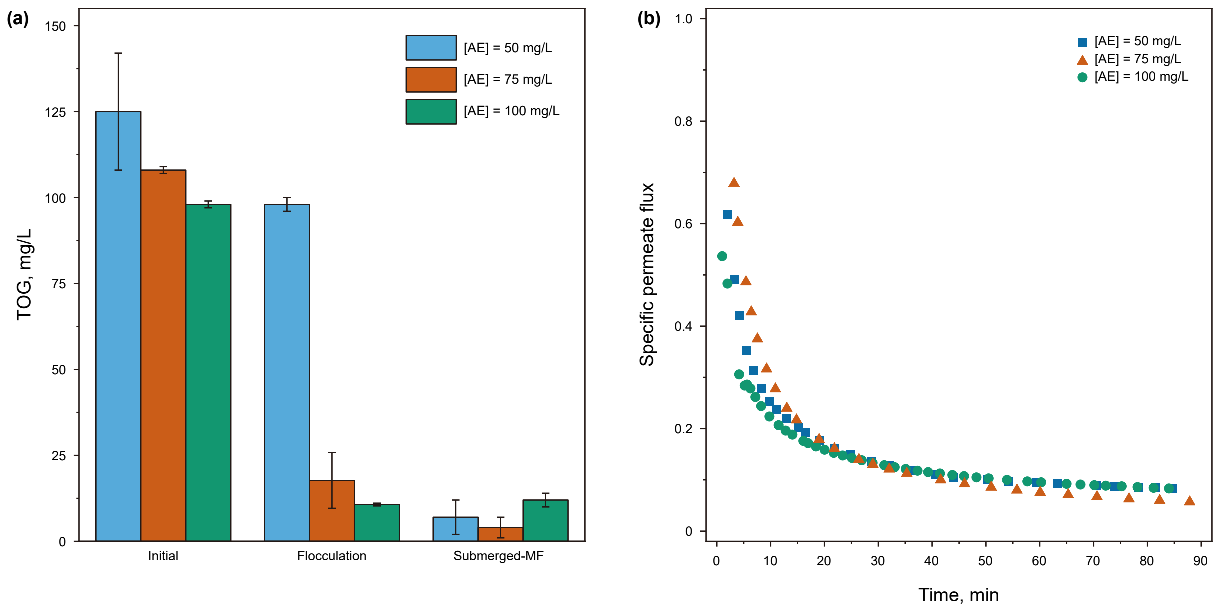


**Fig. 4.** Performance of the integrated flocculation and submerged-MF under different concentrations of coagulant. **(a)** TOG content; **(b)** specific permeate flux of membrane. The SBDS concentration was kept constant at a ratio of 1:2 ([AE]:[SBDS]). See images of SPW-DO samples from each process step in Supplementary Material Fig. S1.

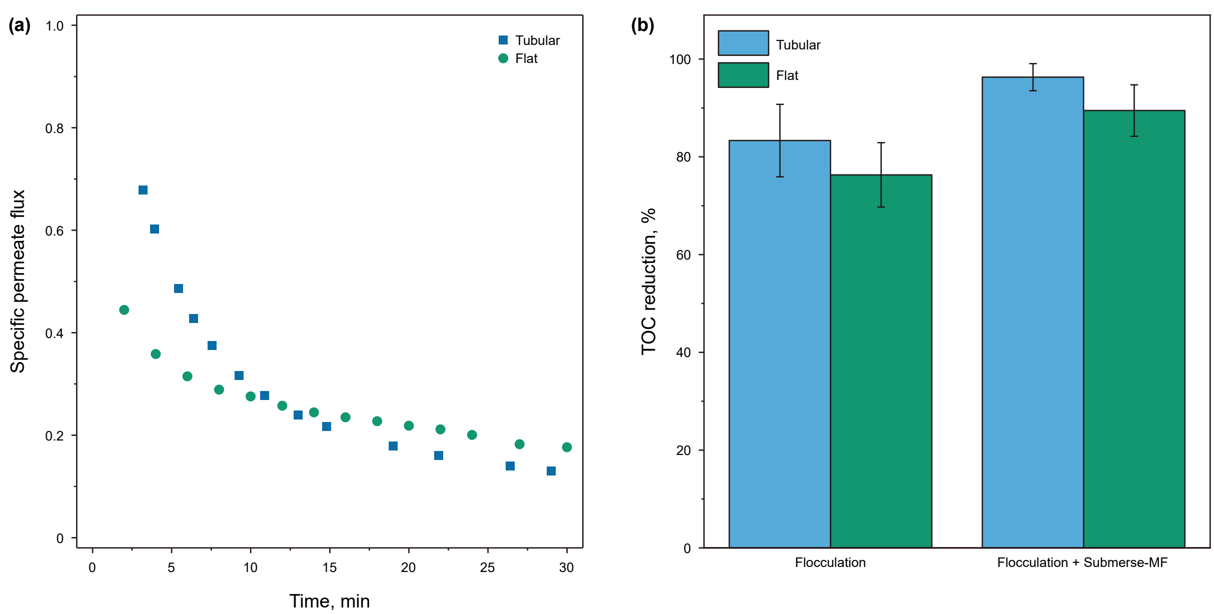


**Fig. 5.** Performance of tubular and flat sheet membrane configurations in the combined treatment of SPW-DO with flocculation followed by submerged-MF. **(a)** Specific permeate flux; **(b)** TOG content.

($m^2$·h) after cleaning, which may indicate more pronounced irreversible fouling or pore blockage.

The superior performance and easier cleaning of the flat sheet membrane are likely attributable to design-related factors. In the tubular membrane configuration, the selective layer is positioned on the internal surface of the channel. Consequently, the flux direction proceeds from the membrane support layer, characterized by a rougher texture and larger pores, toward the selective layer. This arrangement likely favored the accumulation of oil droplets on the external surface of the membrane, contributing to irreversible fouling (i.e., pore blockage). Conversely, in the flat sheet membrane, the feed stream directly contacts the selective layer, which contains pores smaller than the oil droplets. This configuration minimizes the potential for fouling caused by pore blockage. A comparative fouling analysis of the two membrane configurations was conducted via simulation to elucidate the underlying mechanism; the results are detailed in section 3.3.3.

Under identical flocculation conditions (60 °C and 75 mg/L of AE 120), TOG reduction efficiencies were 83% and 76%, yielding final concentrations of 18 ± 8 mg/L and 36 ± 20 mg/L, respectively. In the subsequent submerged-MF step, additional TOG reductions were achieved, consistent with previous observations, resulting in overall removal rates exceeding 89%. Based on the initial TOG concentrations in each test, the specific contribution of the submerged-MF step was 13% for both configurations, corresponding to the retention of approximately 14 mg/L of TOG content by the tubular membrane and 20 mg/L by the flat sheet membrane.

### 3.3.3. Fouling analysis and fluid dynamic simulation

Physicochemical parameters, such as turbidity, TOG concentration, and droplet size, provide a basis for evaluating membrane performance and fouling behavior. The synthetic emulsion (SPW-DO), which exhibits lower turbidity and a narrow droplet size distribution, serves as a model for stabilized oily wastewater under controlled laboratory conditions. In contrast, the real emulsion (OPW-DO), characterized by a broader droplet size distribution and higher contaminant concentrations, more accurately reflects the complexity of oilfield produced water.

These distinct feed properties influence the interaction between oil droplets and membrane surfaces and pores, thereby determining the predominant fouling mechanisms for each membrane configuration. To assess these effects, the experimental flux decline of both tubular and flat membranes was analyzed using Hermia's fouling model in conjunction with a custom Python®-based finite volume simulation. The model-code framework enabled parameter fitting, identification of dominant fouling mechanisms, and comparative evaluation of predictive performance across membrane configurations. Fig. 6 presents the fitting results for both membrane types.

Table 3 provides a summary of the goodness-of-fit, displaying the $R^2$ values for each configuration to demonstrate the model's predictive capability. For the tubular membrane, the permeate flux decline data showed strong agreement with most Hermia models. The complete blocking model yielded the highest correlation ($R^2 = 0.98$), indicating that immediate pore blockage due to particle deposition was the predominant fouling mechanism. The intermediate blocking model also demonstrated a strong fit ($R^2 = 0.97$), suggesting that partial pore constriction and narrowing contributed significantly to fouling, likely resulting from particle accumulation on and within the membrane pores.

The standard blocking model yielded a slightly lower fit, indicating a secondary role of gradual pore narrowing due to adsorbed foulants. In contrast, the cake formation model showed the weakest correlation ($R^2 = 0.83$), implying that external layer accumulation was not the primary fouling mechanism, although it may have contributed in conjunction with pore-blocking phenomena. This combined fouling behavior is typical in oily wastewater and saline feeds containing suspended solids and surfactants, where internal pore interactions and surface deposition occur simultaneously, progressively increasing filtration resistance, especially considering commercial pore sizes ranging from 0.1 to 10 μm (De Bruijn et al., 2005; Field et al., 1995; Hermia, 1985; Ullah et al., 2021; Xiao et al., 2023; Zulkefli et al., 2021).

**Table 3**
Hermia model fit for tubular and flat membranes, based on $R^2$ values.

| | Tubular membrane | Flat membrane |
|---|---|---|
| Standard blockage | 0.89 | Without correlation |
| Complete blockage | 0.98 | Without correlation |
| Intermediate blockage | 0.97 | Without correlation |
| Cake formation | 0.83 | 0.84 |

The flat sheet membrane showed a distinct fouling pattern compared to the tubular setup. In this case, the cake filtration model demonstrated the strongest correlation with the experimental data ($R^2 = 0.83$), indicating that surface deposition and cake layer formation were the primary causes of the flux decline. This finding was experimentally validated (see Fig. S2 in the Supplementary Material). The other models tested exhibited poor fit, often resulting in an $R^2$ values close to zero. This discrepancy does not necessarily reflect model failure; but rather indicates that the underlying assumptions of those models do not align with the physical behavior of the system. These results strongly suggest that under specific operating conditions of this study, the flat sheet membrane is more susceptible to external fouling. Its structural design, featuring horizontal flow channels and a larger exposed surface, facilitates particle accumulatio on the membrane surface, promoting cake layer formation, resulting in flux reduction. The distinct fouling mechanisms observed across membrane configurations carry important implications for fouling mitigation strategies. The flat sheet membrane's susceptibility to cake filtration suggests that optimizing periodic backwashing could be an effective mitigation strategy. Conversely, the predominant issue in the tubular configuration, pore blockage, suggests the need for

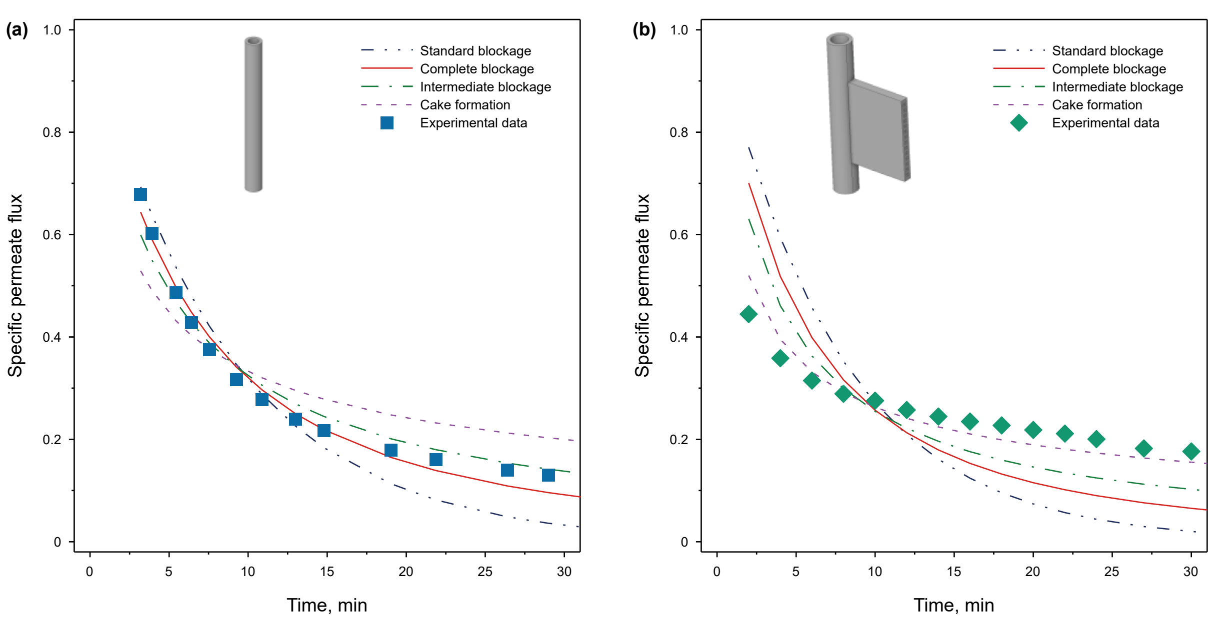


**Fig. 6.** Performance of the Hermia model optimization code for flux analysis for **(a)** tubular membrane and **(b)** flat sheet membrane.

approaches such as chemical cleaning or surface modification to sustain performance.

The Hermia model, originally developed for solid, rigid particles, presents limitations in accurately describing fouling behavior in oil-in-water emulsions (Hermia, 1985). Unlike the model's assumptions, oil exists as deformable droplets capable of coalescing, spreading, and deforming upon contact with the membrane surface. This dynamic behavior, combined with important factors not considered by the model, such as concentration polarization, oil-membrane interactions, and surface tension effects, complicates the fitting of experimental data to any of the four predefined blocking mechanisms. Despite these limitations, the Hermia model can still yield reasonable fits to experimental data under specific conditions. For instance, when a thick, viscous oil layer rapidly forms on the membrane surface, as observed in the flat sheet configuration, the cake filtration mechanism adequately described the process. In such cases, the model serves as a phenomenological descriptor that effectively captures the observed phenomenon of cake formation, even if it does not account for the underlying dynamics of droplet deformation and coalescence. This finding aligns with observations reported by Alborzi et al. (2022).

A comparative analysis of simulation predictions and experimental data for various resistance models from the literature is presented in Fig. 7. The simulated data, generated using the experimental parameters derived from the Hernia models, exhibited notable discrepancies when compared to experimental results. Consequently, the simulated outputs are presented as boxplot diagram for each model (Fig. 7(b) and (d)), allowing comparison of their order of magnitude with the experimental data (Fig. 7(a) and (c)).

Table 4 presents the goodness-of-fit results for the 2D simulated data, comparing the performance of various empirical

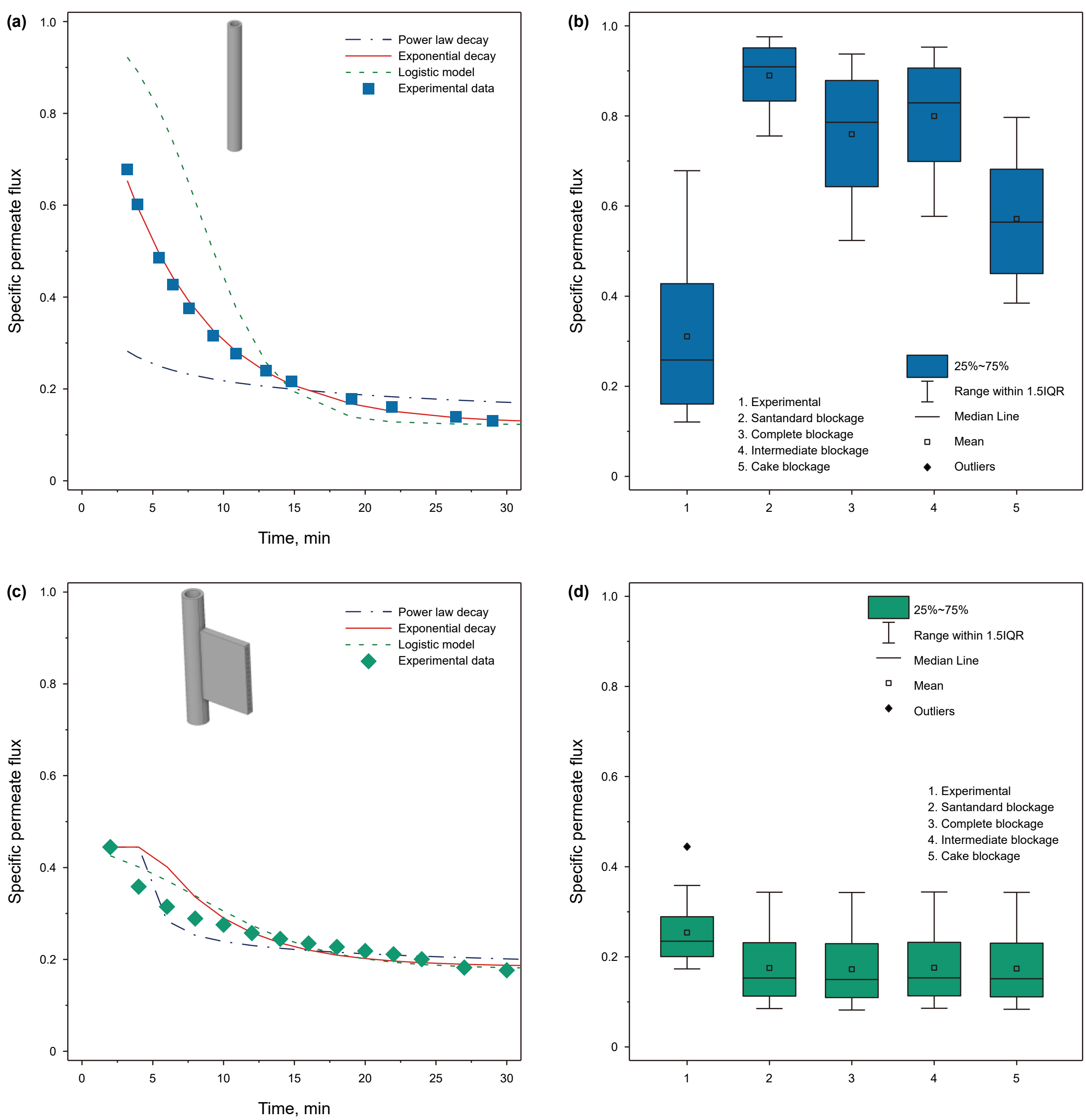


**Fig. 7.** Comparison of experimental data and simulated 2D finite element code for tubular **(a)**–**(b)** and flat **(c)**–**(d)** membranes. Resistance models utilized include power law, exponential, and logistic from literature ((a) and (c)), and Hermia's models ((b) and (d)).

**Table 4**
Analysis of fouling models based on the $R^2$ values of different resistance models, including the Hermia model.

| Model type | | Tubular membrane | Flat sheet membrane |
|---|---|---|---|
| Hermia models | Standard blocking | (−) | (−) |
| | Complete blocking | (−) | (−) |
| | Intermediate | (−) | (−) |
| | Cake filtration | (−) | 0.83 |
| Empirical models | Power law decay | 0.05 | 0.81 |
| | Exponential decay | 0.99 | 0.76 |
| | Logistic model | (−) | 0.87 |

Note: (−) denotes a value below 0.00.

resistance models, including the Hermia model applied in the context of membrane resistances. The model conceptualizes the MF membrane as a region where permeability progressively decreases. This design enables simulation of the entire filtration cycle, from the initial high flux of a clean membrane to the gradual decline induced by fouling. The code architecture allows dynamic adjustment of membrane parameters, including permeability decay rate, delay onset, and species-specific behavior. The resulting flux was fitted to experimental data by optimizing initial permeability and decay rate using a bounded nonlinear optimization routine (*scipy.optimize.minimize*) employing both the 'L-BFGS-B′ and 'TNC' algorithms. This approach produced a strong fit, accurately replicating the sharp initial decline and long-term stabilization observed experimentally.

A comparison between Hermia-based models (Fig. 7(b) and (d)) and empirical decay models (Fig. 7(a) and (c)) reveals distinct behaviors in simulating membrane fouling resistance over time. Although Hermia's flux decay equation resembles exponential decay mathematically, its direct application to resistance fitting yields poor agreement with experimental data. This discrepancy arises because Hermia models describe flux decline via mechanisms such as pore blocking or cake formation, with resistance inferred indirectly from flux measurements. In contrast, exponential decay models represent resistance growth as a direct, empirical, and continuous function, resulting in superior numerical fits. Additionally, Hermia model parameters are interdependent and sensitive to mechanistic assumptions, while exponential and logistic models feature independent parameters and can readily incorporate a resistance floor to replicate the experimentally observed long-term plateau. Thus, while Hermia models are valuable for mechanistic interpretation of fouling, empirical models such as exponential decay offer superior predictive accuracy in discretized flux simulations.

The simulations show marked differences in model performance across membrane systems, emphasizing the critical influence of membrane configuration on fouling dynamics and predictive modeling. For the tubular membrane, the exponential decay model demonstrated the highest predictive accuracy ($R^2 = 0.99$), effectively capturing the sharp initial flux decline. In contrast, the power-law and logistic models performed poorly, with the logistic model producing near-zero $R^2$ values despite its flexibility. This suggests that the simplicity of the exponential model and its focus on early-stage dynamics make it particularly well-suited for this specific configuration. Conversely, simulations for the flat sheet membrane exhibited markedly greater consistency across all resistance models. The logistic decay model provided the best fit to the experimental data, accurately capturing both the steep initial flux decline and subsequent stabilization. The power-law and exponential models also performed reasonably well ($R^2$ values of 0.81 and 0.76, respectively), reflecting general trends in the data although with slight underestimation long-term stabilization.

The improved fit observed for the flat sheet membrane likely results from its simplified geometry, which promotes uniform flow and mild fouling conditions. Such uniformity minimizes spatial heterogeneity arising from complex flow patterns, curvature, and radial gradients inherent to the tubular system. This configuration provides a more predictable, predominantly two-dimensional flow, reducing local variations in transmembrane pressure and concentration polarization. Additionally, simplified geometry enhances numerical stability and spatial resolution within the simulation grid, enabling more accurate coupling between resistance models and flux predictions. Simulations incorporating Hermia's mechanistic models as resistance descriptors further corroborate these findings, as illustrated in Fig. 7(b) and (d). In the flat sheet membrane system, the cake filtration model demonstrated the best performance, with a robust $R^2$ of 0.83. This result suggests that cake formation and intermediate blocking are the dominant fouling mechanisms in this configuration. This contrasts sharply with the tubular membrane, where none of the Hermia-derived models effectively captured the experimental trends. Notably, the empirical logistic decay model, despite lacking a mechanistic basis, achieved predictive accuracy comparable to the Hermia-based cake filtration model. This finding reinforces the practical value of the logistic model for robust empirical fitting, particularly in scenarios where accurate prediction and computational stability are prioritized over a detailed mechanistic interpretation.

The simplified structure and uniform shear environment of the flat sheet membrane promote better alignment with both empirical and mechanistic models. Although mechanistic models such as Hermia's are valuable for elucidating fouling physics, their complexity and susceptibility to instability render simpler, more robust empirical models —such as the exponential and logistic decay—more appropriate for the flat sheet membrane. This fact highlights membrane configuration as a critical factor not only in influencing fouling mechanisms but also in determining the suitability and performance of different modelling approaches.

Given the experimental oil concentration in the emulsion (approximately 150 mg/L), initial oil permeability was set at 45% of the clean water value to reflect partial pore blockage from the beginning of filtration. Fouling onset was delayed by 40 min after the start of filtration, followed by an exponential permeability decline at a rate of $9 \times 10^{-4}$ $s^{-1}$. Permeability ultimately stabilized at 15% of its initial value. This modeling approach successfully replicated both the initial flux decline and the long-term stabilization observed in the experimental data. The estimated oil retention of approximately 74% closely aligned with the experimentally measured rejection of 76% for the SPW-DO system when the logistic resistance model was employed. In comparison, the exponential model produced a lower retention value of 56%. These results support the conclusion that the logistic resistance model offers a more accurate representation of system behavior.

Applying the same approach used for the tubular membrane, the logistic resistance model was implemented for the flat sheet membrane. This approach yielded a calculated oil retention of approximately 84.8%, closely matching the experimentally measured rejection of 86% for this system. By contrast, the exponential model produced a lower retention value of 78%. Thus, a comprehensive data analysis confirms the logistic resistance model as the most suitable option for predicting fouling behavior in flat sheet membrane microfiltration of oil-contaminated solutions, considering the imposed resistance by the setup and stress conditions.

### 3.4. Integration of coagulation/flocculation and membrane separation processes in OPW-DO treatment

Fig. 8 shows the performance evaluation of tubular and flat sheet membrane applied to the combined treatment of OPW-DO, integrating flocculation followed by submerged-MF.

The results demonstrate the combined effectiveness of flocculation and submerged-MF in reducing turbidity and TOG in OPW-DO, replicating the treatment performance previously observed for SPW-DO (synthetic sample) in Section 3.3.1.

The initial sample exhibited elevated turbidity (924 ± 8 NTU) and a TOG concentration (154 ± 22 mg/L). Following flocculation with [AE] at 100 mg/L, turbidity decreased to 398 NTU and TOG to 122 ± 6 mg/L, corresponding to only a 21% TOG removal (Fig. 8(a)). This flocculation performance contrasts with that observed for SPW-DO under identical conditions, where TOG removal ranged from 76% to 84%. The reduced efficiency is likely due to the higher complexity of the real matrix used in OPW-DO, which includes metal ions, hardness (measured at 2.73 g/L), surfactants, and other chemical additives. Such components enhance oil droplet stability, hindering their separation via conventional flocculation (Eftekhardadkhah and Øye, 2013; Gao et al., 2011).

In the subsequent step, submerged-MF with the flat sheet membrane reduced turbidity to 9 NTU and TOG to 1 mg/L, representing complete removal (100%) relative to the initial sample. The tubular membrane achieved comparable efficiency, reducing turbidity to 5.71 NTU and TOG to 1 ± 1 mg/L. These results confirm that both membranes act as robust and effective barriers, even under the high contaminant load presented by OPW-DO. Notably, the final TOG concentrations achieved after filtration were even lower than those observed in SPW-DO tests, highlighting the membranes' capacity to compensate for reduced flocculation efficiency in complex matrices. The observed turbidity reduction further reinforces the overall process efficiency (see Fig. S3 in the Supplementary Material).

The submerged-MF system maintained high performance, likely due to synergistic effects arising from the complex composition of real wastewater, which modified membrane surface interactions. Specifically, the ceramic membrane's intrinsic hydrophilicity was enhanced by the feed's chemical complexity, with dissolved organic compounds modifying interfacial tension. Additionally, particulates may have formed more permeable fouling layers than those observed in synthetic water tests. These combined effects enabled the MF system to compensate for the reduced flotation efficiency while maintaining effective treatment of actual industrial effluent.

Fig. 8(b) illustrates a declining flux trend over time for both membrane configurations, reflecting fouling effects during submerged-MF operation. The tubular membrane exhibited a higher initial flux (1336 L/($m^2$·h)) than the flat sheet membrane (619 L/($m^2$·h)), possibly due to lower hydrodynamic resistance associated with its geometry. However, this configuration was more susceptible to surface fouling, resulting in a sharp flux decline to just 1.4% of the initial value after 90 min. In contrast, the flat sheet membrane demonstrated more stable performance, retaining approximately 3.1% of its initial flux after 100 min of operation.

The flux decline curve indicates that, despite its initial advantage, the tubular membrane experienced more severe fouling, likely due to greater material accumulation on its external surface. This behavior may be attributed to: (i) the convex geometry promoting preferential foulant deposition due to hydrodynamic pressure gradients, and (ii) the larger effective surface area exposed to particulates, increasing the pore blockage probability. This trend is further evidenced by post-cleaning flux recovery: the flat sheet membrane regained 100% of its initial flux, whereas the tubular membrane recovered 32%, indicating more persistent or irreversible fouling, as supported by modeling presented discussed earlier.

Conversely, the flat sheet membrane exhibited a typical polarization layer formation pattern, as evidenced by complete flux

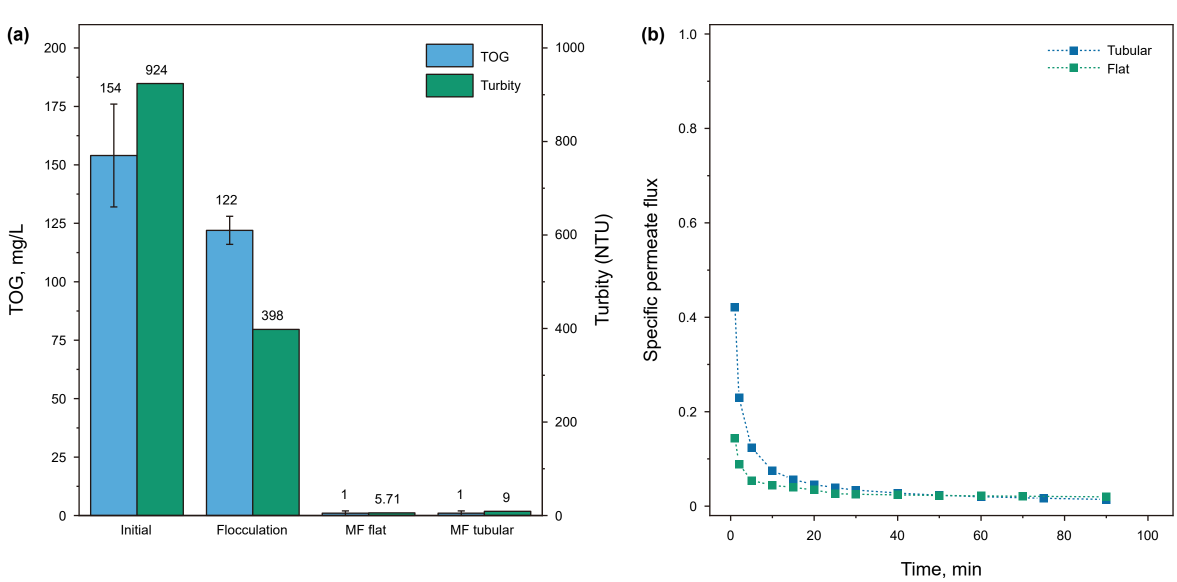


**Fig. 8.** Performance of different membrane configurations in the combined treatment of OPW-DO with flocculation followed by submerged-MF. **(a)** TOG and turbidity; **(b)** Specific permeate flux. See images of OPW-DO samples from each process step in Supplementary Material Fig. S3.

recovery after cleaning. Flux stabilization at similar flux values for both configurations after approximately 30 min suggests the system reached a dynamic equilibrium where: (a) the fouling layer acted as a pre-filter for larger particles, and (b) hydrophilic interactions between the ceramic surface and the complex feed created an effective barrier to oil droplet penetration. This pseudo-steady state explains the comparable performance (>99% oil removal) achieved by both membranes, despite their different fouling mechanisms.

This consistent separation efficiency despite reduced fluxes confirms that membrane performance is primarily governed by the effective pore size following initial fouling layer formation. This phenomenon has critical practical implications, as flat sheet membranes exhibit greater operational resilience due to their reversible fouling behavior, as evidenced by consistent performance with both SPW-DO and OPW-DO. Although enhanced flocculation can enhance permeate flux, the membrane's intrinsic separation capability remains effective even with optimal pretreatment, representing a key advantage for offshore installations dealing with variable produced water compositions.

## 4. Conclusion

This study demonstrated the feasibility of combining flocculation and submerged microfiltration (MF) processes for treating OPW under high salinity and elevated temperature conditions. The integrated system effectively reduced dispersed oil and turbidity in both synthetic and real emulsions, complying with offshore discharge standards (below 30 mg/L), even under suboptimal flocculation performance. A mechanism was proposed for highly saline media, involving partial neutralization or inversion of oil droplet surface charge, which enhances the performance of anionic flocculants in promoting droplet aggregation.

Membrane configuration plays a crucial role in determining fouling behavior. Flat sheet membranes exhibited greater resistance to irreversible fouling and achieved complete flux recovery after cleaning, whereas tubular membranes were more susceptible to pore blockage. Mechanistic modeling using Hermia's approach, combined with empirical resistance simulations, provided insights into fouling dynamics and demonstrated that exponential decay models offer superior accuracy in predicting flux behavior.

From a scientific perspective, this study validates the proof of concept for the combined process (technology readiness level 3), advances understanding of fouling mechanisms in high-salinity oily wastewater treated via MF systems and confirms the utility of integrated modeling tools for predicting flux behavior. From a practical standpoint, the findings support the deployment of modular integrated systems in offshore settings, providing operational flexibility and the adaptability to variable feedwater conditions.

## CRediT authorship contribution statement

**Mariane Carolina Proner:** Writing – original draft, Methodology, Investigation, Conceptualization. **Maria Alice Prado Cechinel:** Writing – original draft, Methodology, Investigation, Conceptualization. **Carine Loureço Alves:** Writing – original draft, Methodology, Investigation, Conceptualization. **Sálvio Lima de Carvalho Neto:** Writing – review & editing, Supervision, Conceptualization. **Silvio Edegar Weschenfelder:** Writing – review & editing, Supervision, Conceptualization. **Sergio Yesid Gómez González:** Writing – review & editing, Supervision, Conceptualization. **Alan Ambrosi:** Writing – review & editing, Supervision, Conceptualization. **Marco Di Luccio:** Writing – review & editing, Supervision, Conceptualization. **Regina de Fátima Peralta Muniz Moreira:** Writing – review & editing, Supervision, Resources, Conceptualization.

## Declaration of competing interest

The authors declare the following financial interests/personal relationships which may be considered as potential competing interests: Regina F. P. M. Moreira reports financial support was provided by Petróleo Brasileiro SA Petrobras. If there are other authors, they declare that they have no known competing financial interests or personal relationships that could have appeared to influence the work reported in this paper.

## Acknowledgments

This work was financially supported by Petróleo Brasileiro S/A (PETROBRAS) – Project EO&M, Process: 2023/00226-0.

## Appendix A. Supplementary data

Supplementary data to this article can be found online at https://doi.org/10.1016/j.petsci.2026.03.025.

## References

Abbasi, M., Sebzari, M.R., Salahi, A., Mirza, B., 2012. Modeling of membrane fouling and flux decline in microfiltration of oily wastewater using ceramic membranes. Chem. Eng. Commun. 199, 78–93. https://doi.org/10.1080/00986445.2011.570391.
Alborzi, A., Hsieh, I.M., Reible, D., Malmali, M., 2022. Analysis of fouling mechanism in ultrafiltration of produced water. J. Water Proc. Eng. 49, 102978. https://doi.org/10.1016/J.JWPE.2022.102978.
Al-Shammari, S.B., Bou-Hamad, S., Al-Tabtabaei, M., 2012. Comparative performance evaluation of microfiltration submerged and pressurized membrane treatment of wastewater. Desalination Water Treat. 49, 26–33. https://doi.org/10.1080/19443994.2012.708194.
Alzahrani, S., Mohammad, A.W., 2014. Challenges and trends in membrane technology implementation for produced water treatment: a review. J. Water Proc. Eng. 4, 107–133. https://doi.org/10.1016/J.JWPE.2014.09.007.
Amakiri, K.T., Canon, A.R., Molinari, M., Angelis-Dimakis, A., 2022. Review of oilfield produced water treatment technologies. Chemosphere 298, 134064. https://doi.org/10.1016/j.chemosphere.2022.134064.
Ariana, A., Cozzarelli, I., Danforth, C., McDevitt, B., Rosofsky, A., Vorhees, D., 2025. Pathways for potential exposure to onshore oil and gas wastewater: what we need to know to protect human health. GeoHealth 9 (4), e2024GH001263. https://doi.org/10.1029/2024GH001263.
Bhattacharya, P., Dutta, S., Ghosh, S., Vedajnananda, S., Bandyopadhyay, S., 2010. Crossflow microfiltration using ceramic membrane for treatment of sulphur black effluent from garment processing industry. Desalination 261, 67–72. https://doi.org/10.1016/J.DESAL.2010.05.029.
Bostick, D.T., 2002. Characterization of Soluble Organics in Produced Water. https://doi.org/10.2172/814231. Oak Ridge, TN (United States).
Dai, P.Y., Liu, Y.Q., Lu, H., Li, Y.D., Yang, Q., 2023. Produced-water treatment: application and research of combined fiber coalescence technique in offshore oilfield. Pet. Sci. 20, 569–576. https://doi.org/10.1016/J.PETSCI.2022.11.013.
De Bruijn, J.P.F., Salazar, F.N., Bórquez, R., 2005. Membrane blocking in ultrafiltration: a new approach to fouling. Food Bioprod. Process. 83, 211–219. https://doi.org/10.1205/FBP.04012.
Dudek, M., Øye, G., 2018. Microfluidic study on the attachment of crude oil droplets to gas bubbles. Energy & Fuels 32, 10513–10521. https://doi.org/10.1021/acs.energyfuels.8b02236.
Eftekhardadkhah, M., Øye, G., 2013. Correlations between crude oil composition and produced water quality: a multivariate analysis approach. Ind. Eng. Chem. Res. 52, 17315–17321. https://doi.org/10.1021/ie4028457.
Field, R.W., Wu, D., Howell, J.A., Gupta, B.B., 1995. Critical flux concept for microfiltration fouling. J. Membr. Sci. 100, 259–272. https://doi.org/10.1016/0376-7388(94)00265-Z.
Gao, B., Jia, Y., Zhang, Y., Li, Q., Yue, Q., 2011. Performance of dithiocarbamate-type flocculant in treating simulated polymer flooding produced water. J. Environ. Sci. 23, 37–43. https://doi.org/10.1016/S1001-0742(10)60370-1.
Georgie, W., 2024. Maxoil training course: the science and technology of water management in upstream operation. In: SPE Training Course. SPE (Society of Petroleum Engineers).
Hermia, J., 1985. Blocking filtration. Application to non-newtonian fluids. NATO ASI Ser., Ser. E 83–89. https://doi.org/10.1007/978-94-009-5091-7_5.
Hu, B., Huang, L., Chang, H., Ji, Z., Yan, Z., Qu, D., Wang, J., Qu, F., Liang, H., 2025. A review of key parameters affecting inorganic scaling in thermal, pressure,

and osmosis-driven membranes for produced water desalination. Sep. Purif. Technol. 354, 129023. https://doi.org/10.1016/j.seppur.2024.129023.

Huang, B., Li, X., Zhang, W., Fu, C., Wang, Y., Fu, S., Huang, B., Li, X., Zhang, W., Fu, C., Wang, Y., Fu, S., 2019. Study on demulsification-flocculation mechanism of oil-water emulsion in produced water from Alkali/Surfactant/polymer flooding. Polymers 2019 11, 11. https://doi.org/10.3390/POLYM11030395.

Jiménez, S., Micó, M.M., Arnaldos, M., Medina, F., Contreras, S., 2018. State of the art of produced water treatment. Chemosphere 192, 186–208. https://doi.org/10.1016/J.CHEMOSPHERE.2017.10.139.

Jin, X., Wang, W., Wang, S., Jin, P., Wang, X.C., Zhang, W., An, W., Wang, Y., 2019. Application of a hybrid gravity-driven membrane filtration and dissolved ozone flotation (MDOF) process for wastewater reclamation and membrane fouling mitigation. J. Environ. Sci. 81, 17–27. https://doi.org/10.1016/J.JES.2019.02.011.

Khan, N., Brettmann, B., Khan, N., Brettmann, B., 2018. Intermolecular interactions in polyelectrolyte and surfactant complexes in solution. Polymers 2019 11, 11. https://doi.org/10.3390/POLYM11010051.

Kim, D., Livazovic, S., Falca, G., Nunes, S.P., 2019. Oil–water separation using membranes manufactured from cellulose/ionic liquid solutions. ACS Sustain. Chem. Eng. 7, 5649–5659. https://doi.org/10.1021/acssuschemeng.8b04038.

Li, Y., Jiang, H., Wu, Y., Zhu, H., Liu, Y., Lu, H., Liu, B., Yang, Q., 2025. Microbubbles enhance oil-in-water emulsion separation in fibrous coalescers. Water Res. 268, 122573. https://doi.org/10.1016/j.watres.2024.122573.

Liu, Y., Lu, H., Li, Y., Xu, H., Pan, Z., Dai, P., Wang, H., Yang, Q., 2021. A review of treatment technologies for produced water in offshore oil and gas fields. Sci. Total Environ. 775, 145485. https://doi.org/10.1016/J.SCITOTENV.2021.145485.

Motta, A., Borges, C., Esquerre, K., Kiperstok, A., 2014. Oil produced water treatment for oil removal by an integration of coalescer bed and microfiltration membrane processes. J. Membr. Sci. 469, 371–378. https://doi.org/10.1016/J.MEMSCI.2014.06.051.

Padaki, M., Surya Murali, R., Abdullah, M.S., Misdan, N., Moslehyani, A., Kassim, M.A., Hilal, N., Ismail, A.F., 2015. Membrane technology enhancement in oil–water separation. A review. Desalination 357, 197–207. https://doi.org/10.1016/j.desal.2014.11.023.

Pereira, G.L.D., Cardozo-Filho, L., Jegatheesan, V., Guirardello, R., 2023. Generalization and expansion of the hermia model for a better understanding of membrane fouling. Membranes 13, 290. https://doi.org/10.3390/membranes13030290.

Piccioli, M., Aanesen, S.V., Zhao, H., Dudek, M., Øye, G., 2020. Gas flotation of petroleum produced water: a review on status, fundamental aspects, and perspectives. Energy & Fuels 34, 15579–15592. https://doi.org/10.1021/acs.energyfuels.0c03262.

Piombini, C.R., Silva, L.L.S., Da Fonseca, F.V., Campos, J.C., 2021. Submerged microfiltration membrane and activated carbon processes for recalcitrant compounds removal in oil refinery effluent as electrodialysis pre-treatment. Water Sci. Technol. 84, 1403–1416. https://doi.org/10.2166/WST.2021.318.

Scharnberg, A.R.A., Oliveira, H.A., Weschenfelder, S.E., Rubio, J., Azevedo, A.C., 2023. Flocculation of emulsified oil-in-water with dodecylbenzene sulfonate and polyacrylamide and floc separation by dissolved air flotation. Colloids Surf. A Physicochem. Eng. Asp. 669, 131496. https://doi.org/10.1016/J.COLSURFA.2023.131496.

Shahrim, N.A., Abounahia, N.M., El-Sayed, A.M.A., Saleem, H., Zaidi, S.J., 2023. An overview on the progress in produced water desalination by membrane-based technology. J. Water Proc. Eng. 51, 103479. https://doi.org/10.1016/j.jwpe.2022.103479.

Shim, J., Koo, J.-W., Hwang, T.-M., Sul, J.-H., Jeong, S., 2025. Integrated micro/nano bubbles-assisted induced gas flotation and ceramic membrane filtration for chemical-free treatment of oil sands process-affected water. Sep. Purif. Technol. 374, 133736. https://doi.org/10.1016/j.seppur.2025.133736.

Sutzkover-Gutman, I., Hasson, D., Semiat, R., 2010. Humic substances fouling in ultrafiltration processes. Desalination 261, 218–231. https://doi.org/10.1016/J.DESAL.2010.05.008.

Taghizadeh Mohammadi, M.J., Movahedirad, S., 2024. A digital image analysis approach to understand the microscopic and macroscopic phenomena in dissolved air flotation. Sci. Rep. 14, 14381. https://doi.org/10.1038/s41598-024-65325-5.

Tian, J., Wang, L., Ni, L.P., Mou, L.W., Su, S. Te, Ostadhassan, M., 2023. Temporal variations in geochemistry of hydraulic fracturing fluid and flowback water in a tight oil reservoir. Pet. Sci. 20, 3013–3021. https://doi.org/10.1016/J.PETSCI.2023.05.004.

Ullah, A., Tanudjaja, H.J., Ouda, M., Hasan, S.W., Chew, J.W., 2021. Membrane fouling mitigation techniques for oily wastewater: a short review. J. Water Proc. Eng. 43, 102293. https://doi.org/10.1016/J.JWPE.2021.102293.

Wang, C., Lü, Y., Song, C., Shi, J., Zhang, P., He, L., 2023. Microbubbles preparation by partial vaporization of low boiling condensate for crude oil/water separation. J. Water Proc. Eng. 53, 103625. https://doi.org/10.1016/j.jwpe.2023.103625.

Wang, C., Lü, Y., Song, C., Zhang, D., Rong, F., He, L., 2022. Separation of emulsified crude oil from produced water by gas flotation: a review. Sci. Total Environ. 845, 157304. https://doi.org/10.1016/J.SCITOTENV.2022.157304.

Xiao, T., Zhu, Z., Li, L., Shi, J., Li, Z., Zuo, X., 2023. Membrane fouling and cleaning strategies in microfiltration/ultrafiltration and dynamic membrane. Sep. Purif. Technol. 318, 123977. https://doi.org/10.1016/J.SEPPUR.2023.123977.

Yang, R., Li, H., Huang, M., Yang, H., Li, A., 2016. A review on chitosan-based flocculants and their applications in water treatment. Water Res. 95, 59–89. https://doi.org/10.1016/j.watres.2016.02.068.

Zhang, H., Xu, M., Chen, M., Cui, Y., Chen, L., Dai, X., Dai, J., 2022. Fabrication of high flux porphrin-cored with siloxane-poly(amido amine) dendrimer/PVDF composite membrane for oil/water separation and dye degradation. J. Environ. Chem. Eng. 10, 107634. https://doi.org/10.1016/j.jece.2022.107634.

Zhao, C., Zhou, J., Yan, Y., Yang, L., Xing, G., Li, H., Wu, P., Wang, M., Zheng, H., 2021. Application of coagulation/flocculation in oily wastewater treatment: a review. Sci. Total Environ. 765, 142795. https://doi.org/10.1016/j.scitotenv.2020.142795.

Zolfaghari, R., Fakhru'l-Razi, A., Abdullah, L.C., Elnashaie, S.S.E.H., Pendashteh, A., 2016. Demulsification techniques of water-in-oil and oil-in-water emulsions in petroleum industry. Sep. Purif. Technol. 170, 377–407. https://doi.org/10.1016/J.SEPPUR.2016.06.026.

Zulkefli, N.F., Alias, N.H., Jamaluddin, N.S., Abdullah, N., Manaf, S.F.A., Othman, N.H., Marpani, F., Mat-Shayuti, M.S., Kusworo, T.D., 2021. Recent mitigation strategies on membrane fouling for oily wastewater treatment. Membranes 12 (1), 26. https://doi.org/10.3390/membranes12010026.